Real-time analysis of polymer flow under real processing conditions applied to microinjection molding

Julien Giboz, Florence Dubelley, S. Carrier, L. Tenchine, Y. Molmeret, Patrice Mele

Version of Record: https://www.sciencedirect.com/science/article/pii/S1526612522000470
Manuscript_1151080c6d7ab85d083ff1dec8241451

Real-time analysis of polymer flow under real processing conditions applied to microinjection molding

J. Giboz[1], F. Dubelley[1,2], S. Carrier[1], L. Tenchine[2], Y. Molmeret[2], P. Mele[1]

[1] Univ. Grenoble Alpes, Univ. Savoie Mont Blanc, CNRS, Grenoble INP*, LEPMI, 38000 Grenoble, France
* Institute of Engineering Univ. Grenoble Alpes

[2] IPC - Centre Technique Industriel de la Plasturgie et des Composites, Bellignat, France

Highlights

- New method is presented to analyze the real flow behavior in thin-wall molding.
- The flow behavior shows size effects with the thickness decrease.
- Flow rates and pressure drops decrease with the thickness, following power laws.
- The mold temperature has no influence for thicknesses > 0.4mm.
- Under a thickness yield $h_{critical}$ of 0.4mm, an intensified energy dissipation occurs.

Graphical Abstract

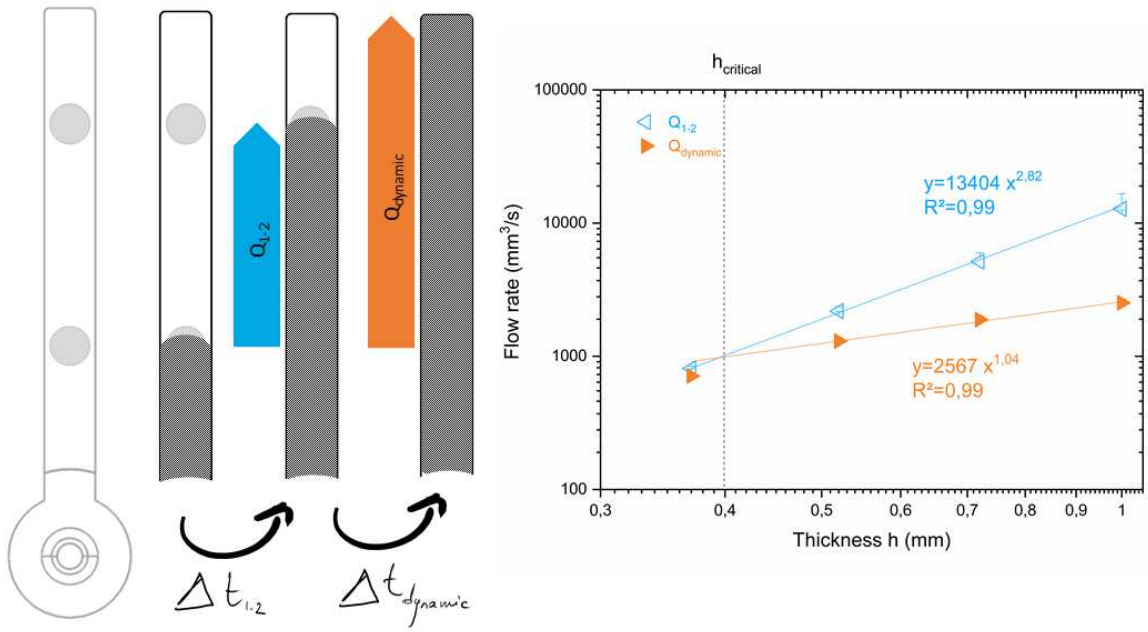

Abstract

This study is about the size effects in thin-walled injection molding: it was carried out from the rheological analysis of a commercial copolymer measured in cavities of various thicknesses ranging from 1 mm to 0.37 mm. A specific analysis of the in-situ cavity pressure evolution based on the derivative of the pressure signals give valuable information about the complex mechanisms of polymer flow in real processing conditions. The results show that a decrease of the cavity thickness leads to antagonistic effects on the rheological behavior, with (i) an increase of the pressure losses and (ii) a decrease of the volume flow rates according to a power law. A specific behavior was also observed for the thinnest cavity (0.37 mm) where the pressure drops are amplified, not following the previous power law and a temperature rise without equivalent. To understand this result, a specific study on the influence of the mold temperature was performed, highlighting again the different behavior of the polymer flow within the thinner cavity. It was revealed that this phenomenon of thermal or energetic dissipation obeys an Arrhenius law, partly explaining the strong pressure drops observed.

Keywords

Injection molding, surface effects, thin-wall molding, in-situ rheological behavior, Ethylen-Norbornen block copolymer

1 Introduction

An ongoing challenge addressed to the plastic industry is to reduce the manufacturing costs or add new functionalities to products [1]. The manufacturing replication process of microinjection molding (µIM) have enabled the mass production of lighter, thinner, and smaller devices for applications within healthcare, automotive, communication and consumer electronics sectors [2]. The trend is to provide new products with enhanced properties by replicating the shapes and structures of the tool onto their surfaces directly by molding micro or nanotextures [3]. It is established that the injection molding phase involves large mechanical and thermal gradients, amplified when the dimensions of the objects or textures are lowered [4 5]. The design and the processing conditions can also accentuate these gradients and alter the final properties of the parts or the polymer [6,7]. Therefore, the design must be adapted to the dimensions of the objects, because their manufacturability depends on the desired ratio between the flow length (L) to the smallest cavity height (h). For example, in isothermal conditions, Yao et al. [8] have shown that a linear relationship exists between the cavity aspect ratio (L/h) and the pressure drops within flow (ΔP), with higher slopes for cold filling conditions (T_{melt} = 265°C for a polycarbonate and T_{mold} = 120°C) compared to isothermal conditions (T_{melt} = T_{mold} =265°C). These authors also showed that the maximum achievable flow length corresponds to a ratio L/h = 240 whatever the thickness of the cavity, in these isothermal conditions.

For real injection molding conditions, where complex thermal and mechanical mechanisms occur along the flow path, Mele and Giboz demonstrated that pressure drops in cavities lower than 1 mm thick increase with the square of the aspect ratio L/h, regardless of the molding conditions [9]. Furthermore, the non-Newtonian rheological behavior of polymers is directly related to the shear rate, which is amplified in small cavities. Vasco et al., for example, observed a transition from a fountain flow to a plug flow for critical shear rates above 5000 s^{-1}, values measured for a microchannel of 200 × 200 µm and about 9000 s^{-1} for a microchannel of 400 × 100 µm [10]. These results were confirmed by Deng et al., who showed by capillary rheometer (die Ø0.2 mm) and under isothermal conditions that plug flow intensity increases as wall-slip appears, for three different polymers like polyurethane, polystyrene, and polypropylene [11]. The authors attribute the plug flow transition to a "slip" at the mold wall due to disentanglement between macromolecular chains in the adhesion zone and the free mass zone. Sorgato et al. also report a decrease in pressure with the occurrence of wall slip [12], confirmed recently by Trotta et al. [13]. The authors have reported that a viscosity reduction exists within a polymer flow 400µm thick cavity, due mostly to wall slip (at the surface) and a possible contribution of both viscous dissipation and polymer compressibility (in the volume). These interesting results point out that an in-depth analysis must be conducted to better detail the different influential parameters, mainly based on the pressure signal measurements and the data processing (difference of pressure ΔP). For this reason, a specific attention must be paid to the signal processing and the variations observed, to draw solid conclusions about their meanings. [9].

Moreover, the reduction of the size of the parts and the cavity thicknesses accentuates the physical and chemical phenomena taking place over the surface of the parts: as the surface/volume ratio increases, the effects arising at the interface between the mold and the polymer flow are thus reinforced because of specific thermal and mechanical conditions. Vera et al. studied the effect of the surface tension between the polymer and various coatings applied on a steel surface; they concluded that the higher the works of adhesion between polymer/mold, the better the replication rate [14], results confirmed by Zhang et al. [15]. Additionally, Masato et al. showed for a melted polystyrene that the better the polymer wettability, the lower the pressure drop within the flow. Indeed, the authors report a linear relationship between the contact angle of the polymer melt and the surface energy, changed thanks to various coatings [16]. The surface roughness should also be considered in this analysis, as it can influence the rheological behavior, as reported by Surace et al [17]. These authors have indeed shown that the flow length increases both with (i) the surface roughness of the mold and (ii) the contact angle between the polymer in the melted state and the cavity surface. Higher values of surface roughness or contact angle between the two materials increase the amount of air trapped between the surface asperities, which leads to a significant

reduction in the cooling rate and the adhesion of the polymers to the wall, explaining then, according to the authors, the longer flow length observed.
The study of the rheological behavior of polymers under real injection conditions has been the subject of various studies, using high-speed cameras in different wavelength spectra (infrared or visible) or using temperature and pressure sensors (T & P) implanted directly in the cavity [13,18,19,20]. If high-speed cameras allow a direct visualization of the polymer flows, the use of T & P sensors allows in-situ monitoring of the evolution of state variables [21]. The complexity of using these sensors as probes in microinjection molding processes are increased, because of the short cycle times (the filling phase being carried out in a few hundreds of milliseconds), the very strong variations of pressure and the high speeds of the polymer flows, the important thermal and mechanical gradients, and most of all, the design and realization of sensor housing, requiring tolerances in the micron range [13]. To do so, an instrumented mold, called “La Rotonde”, was developed specifically to study the polymer flow behavior as a function of the cavity thickness and the cavity temperature [9]. This paper presents an original method of reprocessing the pressure and temperature signals, making one able to define exactly the transition from a dynamic flow during cavity filling to a static packing of the polymer, and use the concomitant pressures values. This is based on the variation of the pressures in the cavity and on the calculation of its temporal first derivative. The experiments address first the variation of the polymer rheology (Pressure drop, flow speed and rate) in cavities of various thicknesses and are completed by the analysis of its temperatures variation within the cavities.

2 Experimental section

2.1 Part design and in-situ measurements

A specific experimental device, named “La Rotonde”, was developed to produce thin-walled parts of different thicknesses by injection molding. The dimensions of the micro-parts were 45 x 5 x h mm^3 of parallelepiped shape, presented in Fig. 1, a. Four cavities with various heights h were studied, ranging from 1000 to 370 µm, according to a constant step logarithmic decay, with ratios L/h allowing a complete filling of the cavities [9]. One mold insert includes the four cavities, placed in the moveable half of the mold. The insert can be rotated and aligned with the sensors located in the fixed mold half (Fig. 1, right). This allows a rapid change of the thickness configuration (not much than 1 minute) without long or complex manipulation, and without disturbing much the local molds and inserts temperatures.

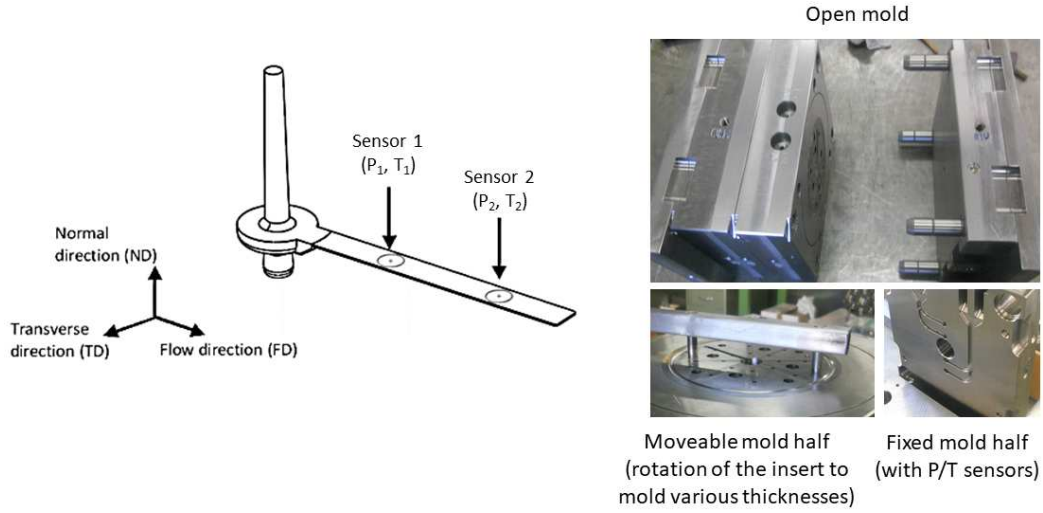

Figure 1 : Part design and pressure & temperature sensor’s locations (left) and “La Rotonde” mold (right).

The in-situ pressure and temperature measurements are done thanks to two coupled sensors measuring pressure & temperature (∅4mm, Kistler® 6190CA). These are connected to a signal conditioner Kistler® 2859 including charge and thermocouple amplifiers (Type 5727 and 2207 respectively, 4-channels). An additional voltage amplifier has been also used to follow the 0-10V signals of the machine and mold variables (injection molding pressure, temperatures of the mold halves). Dataflow software (V2.5) was the interface used to set up the data collection, the different sensors and board characteristics, the frequency, the variable followed and the data processing. The two sensors are located along the flow path respectively at 12.5mm (sensor 1, measuring P_1 and T_1) and 32.5mm (sensor 2, measuring P_2 and T_2) from the injection gate (Figure 1, left). During the molding phase, the data acquisition system simultaneously recorded the pressures and temperatures given by the two sensors (P_1, T_1, P_2, T_2) synchronously with the injection pressure of the machine (P_{inj}) during the molding cycles. An inductive proximity sensor detects the mold closing, which was used to trigger the data measurement at a sampling frequency of 500Hz. The reported data are averaged values over 10 cycles and were recorded once the pressure and temperature signals were stable for each condition, i.e. after more than 10 molding cycles to reach stable processing conditions.

2.2 Polymer and molding conditions

The polymer chosen in this study is a thermoplastic Cyclo-Olefin Copolymer (COC), i.e. a Ethylen-Norbornen block copolymer, provided by Topas, grade 5013. The ratio of the constitutive

Ethylen-Norbornen units by weight is 23/77. The average molecular weights are $M_n = 31.10^3$ g.mol^{-1} and $M_w = 76.10^3$ g.mol^{-1}, and the glass transition temperature $T_g = 134°C$. This copolymer was chosen for its low viscosity (Melt Volume Rate = 48 cm^3/10min), favoring the filling of thin wall cavities [22]. The molded parts were produced with an electric injection molding machine (Engel Victory ECV 80/50) equipped with a 22 mm diameter screw. The molding conditions were defined to mold complete parts for all studied thicknesses.

- A first set of experiments has been conducted with the molding conditions given in Table 1, at a mold temperature of $T_{mold} = 120°C$, to analyze the flow behavior in cavities of various thicknesses.
- Then, a second set of experiments has been conducted in the same way, but with various mold temperatures, in the range of $30°C < T_{mold} < 120°C$. The molding parameters are shown in Table 1.

Different packing steps had to be used for process stability issues and to limit mechanical stresses within injection molding machine components. Indeed, the high speeds and pressures set can lead to unprecise screw movements control, especially at the V/P switchover. For this reason, three packing steps were used for the thickness 0,72mm, 0,52 and 0,37mm (Table 1). For the 1mm thick parts, these packing conditions involved too high internal stresses, involving part defects during demolding. The problem has been solved by reducing the packing pressures, without varying the packing time.

Table 1 : Process conditions used for the parts molding.

Melt temperature (°C) T_{inj}		280	
Mold temperature (°C) T_{mold}		120, 90, 60, 30	
Injection rate (cm^3/s)		70	
Max injection pressure (MPa) P_{inj}		125	
Packing steps	Cavity	1 mm	0.37, 0.52, 0.72 mm
	$P_{packing-1}$ (MPa)	40	100
	$t_{packing-1}$ (s)	4.5	4
	$P_{packing-2}$ (MPa)	10	60
	$t_{packing-2}$ (s)	2.5	0.5
	$P_{packing-3}$ (MPa)		50
	$t_{packing-3}$ (s)		2.5

3 Results and discussion

3.1 New method for analyzing the dynamic behavior of the polymer flow, based on the first order derivative of *in-situ* pressure over time.

3.1.1 Ex-situ and in-situ pressure evolution with time

The Figure 2 shows the time evolution of the machine injection pressure during the dynamic filling step (t < 0.25s); the following step being the packing phase, not reported here, as the pressures were almost constants from 0.25s to 14s. The figure shows an example of the variations of the ex-situ injection pressure (P_{inj}) and the cavity pressures, called "in-situ" (P_1, T_1 & P_2, T_2), for a mold temperature of 120°C, in the case of the 0.37mm thick cavity.

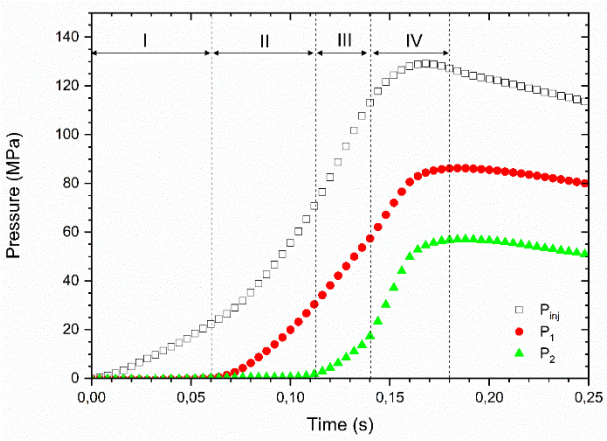

Figure 2: Typical pressure signals recorded for the 0.37 mm with a mold temperature of 120°C, with injection pressure P_{inj}, and local pressure measured with sensor 1 named (P_1) and sensor 2 named (P_2), during the filling phase.

The injection pressure P_{inj} first shows a clear increase during phase I, which corresponds to the pressure needed to fill the sprue (36 mm long) and the first part of the cavity located before sensor 1. Then, the injection pressure increases continuously to reach the maximum pressure set to 125 MPa in 0.17s. During this time, the pressure signals highlight several phases. The phase II shows a rise of the pressure signals P_1, due to flow front progression until sensor 2. When the flow reaches the P_2 sensor location, marking the beginning of phase III, P_2 increases with an almost similar time dependance than P_1. Finally, P_2 reaches a maximum during phase IV; this maximum value appearing almost simultaneously with the highest values of the signals of P_1 and P_{inj}.

These concomitant highest values indicate that cavity filling is fully completed, with corresponding pressures called hereinafter $P_{1_{max}}$ and $P_{2_{max}}$. At that time, the polymer does not flow anymore. For this reason, the maximum pressures are reached for "static" conditions. In the literature, these values are considered as the pressures to be used for calculating the pressure drops under real processing conditions[10,13,20], but seems to be the signature of the packed polymer more than the pressure inside the moving polymer flow, in a "dynamic state". In the following part, a thorough study considering the temporal variations of these intra-cavity signals give issues about their significance, and the link with the "dynamic" state of the polymer flow during filling and the "static" state reached once the cavity is filled.

3.1.2 Analysis of cavity filling kinetics from time-related variations of pressure signals

The new method proposed to deeper analyze the flow behavior is based on the calculation of the first derivative of the pressure signals as a function of time, dP_1/dt and dP_2/dt, plotted in Figure 3a (identified by P'_1 and P'_2 respectively). The numerical calculation of the signals' derivatives has been done for each time step *j*, as follows:

$$\frac{dP_1}{dt} = \frac{P_{1_{j+1}} - P_{1_j}}{t_{j+1} - t_j} \quad \text{and} \quad \frac{dP_2}{dt} = \frac{P_{2_{j+1}} - P_{2_j}}{t_{j+1} - t_j} \tag{1}$$

The Figure 3a presents the calculated derivatives and the corresponding pressure signals, with a common time scale. Both were considered to analyze the flow dynamic, which is not reported elsewhere in the literature. With this representation, several mechanisms can be detected during the filling phase, with the presence of several peaks, characteristics of the flow front behavior, schemed in Figure 3b, with:

- the beginning of the pressure rise, the flow front reaches the sensor 1, as schematized in Figure 3b;
- the arrival of the flow front at sensor 2 leading to the presence of a new shoulder or an additional peak whose intensity can vary, also schemed in Figure 3b;
- a simultaneous increase of the two pressure signals, which reach their maximum values, equal to respectively $P'_{1_{max}} = 1200$ MPa/s and $P'_{2_{max}} = 1700$ MPa/s. The coincidence of these two maximum values at the same time can only be related to the presence of an obstacle in front of the flow, thus explaining these synchronous rises, which can be attributed to the arrival of the flow at the end of the cavity.

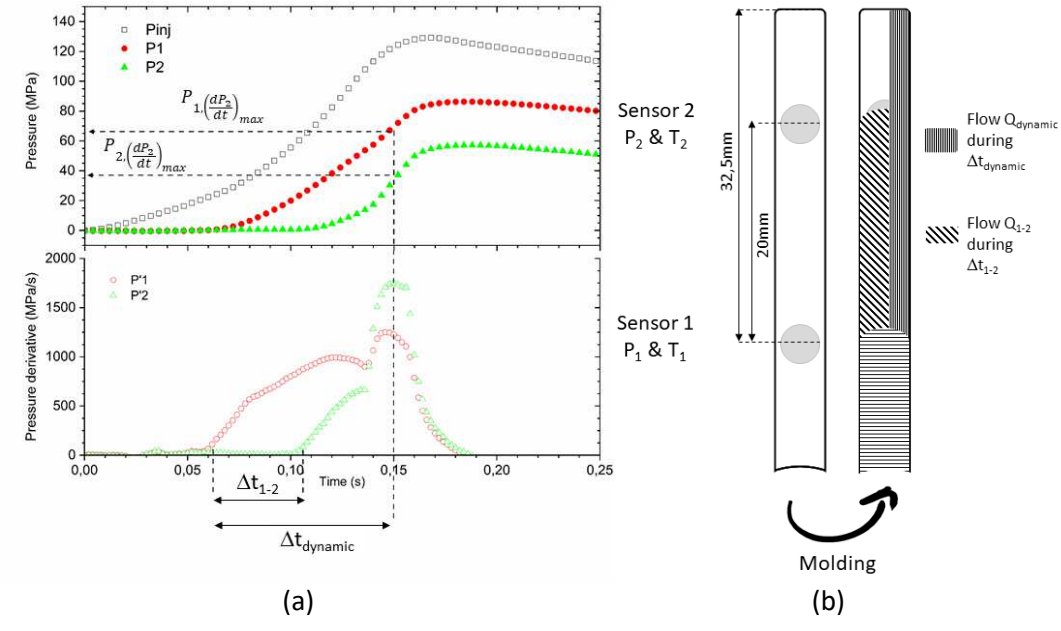

Figure 3 : a) Pressure signal against time during the filling phase, given by the P_1 and P_2 sensors, and their derivatives P'_1 and P'_2 respectively (example given for 0.37mm and T_{mold} = 120°C) with the definition of the different parameters for the study: $P_{1,(P'2)max}$, $P_{2,(P'2)max}$, $\Delta t_{1\text{-}2}$, $\Delta t_{dynamic}$. b) Scheme of the flow front gradually filling the cavity, and definition of the different times and flow considered.

This analysis shows that the polymer flow is in a dynamic state until the simultaneous appearance of the maximum of the derivatives, for a time called $\Delta t_{dynamic}$

Thus, the values of pressures $P_{1,\left(\frac{dP_2}{dt}\right)_{max}}$ and $P_{2,\left(\frac{dP_2}{dt}\right)_{max}}$ (called $P_{1,(P'2)max}$ and $P_{2,(P'2)max}$ in the text, respectively), can be determined and used to calculate the pressure drop $\Delta P_{dynamic}$ according to equation (2).

$$\Delta P_{dynamic} = P_{1,\left(\frac{dP_2}{dt}\right)_{max}} - P_{2,\ \left(\frac{dP_2}{dt}\right)_{max}} \quad (2)$$

- The time $\Delta t_{1\text{-}2}$ corresponds to the time required for the polymer flow to travel the 20mm length between the two sensors and are calculated from equation (3). The contact of the polymer flow with the sensor is defined when the pressure variation reaches 0.4 MPa in 2ms (corresponding to $dP_2/dt = dP_1/dt = 200$ MPa/s, the sensor background being +/- 0.1 MPa). The flow time $\Delta t_{1\text{-}2}$ is then obtained using:

$$\Delta t_{1-2} = t_{\left(\frac{dP_2}{dt}\right)_{=200}} - t_{\left(\frac{dP_1}{dt}\right)_{=200}} \quad (3)$$

- The second time $\Delta t_{dynamic}$ is the time required for the polymer flow to reach the end of the cavity from sensor P1; it is obtained using (4):

$$\Delta t_{dynamic} = t_{\left(\frac{dP_2}{dt}\right)_{max}} - t_{\left(\frac{dP_2}{dt}\right)_{>200}} \quad (4)$$

From these two flow times and knowing the two lengths in the cavities, two flow velocities can be calculated using equations (5 and 6) and allow to estimate the two flow rates, Q_i, according to equations (7 and 8):

$$v_{1-2} = \frac{\Delta l_{1-2}}{\Delta t_{1-2}} \quad (5) \qquad v_{dynamic} = \frac{\Delta l_{1-End}}{\Delta t_{dynamic}} \quad (6)$$

And

$$Q_{1-2} = \frac{S.\Delta l_{1-2}}{\Delta t_{1-2}} \quad (7) \qquad Q_{dynamic} = \frac{S.\Delta l_{1-End}}{\Delta t_{dynamic}} \quad (8)$$

With S: the cross-sectional area, $\Delta l_{1\text{-}2} = 20$ mm, the distance between the two sensors centers, $\Delta l_{1\text{-}End} = 32.5$ mm, the distance between the sensor 1 center and the end of the cavity (Figure 3b).

3.2 Evolution of the rheological behavior of polymers as a function of cavity thickness

The Figure 4a shows the evolution of the different maximum pressure values during the dynamic filling of the cavity *vs.* the different thicknesses. Here, P_{inj} is the highest compared to $P_{1,(P'2)max}$, due to pressure loss within the feeding channels. No variation of this first parameter can be observed with the decrease in thickness. On the contrary, a gradual pressure loss with the reduction of thickness is revealed on the sensor 2 position. This decrease is accentuated for the 0.37mm cavity, where a very strong decrease of $P_{2,(P'2)max}$ occurs. Figure 4b shows the evolution of $\Delta P_{dynamic}$ as a function of the thickness of the cavity. As previously noted [9], the decrease of the cavity thickness leads to a strong increase of the dynamic pressure drops, following the power law:

$$\Delta P_{dynamic} = a\, h^{-b} \quad (9)$$

With a = pre-factor, h = thickness and b = exponent expressing the slope of the pressure variation with the thickness. The value given are calculated for 10 cycles.

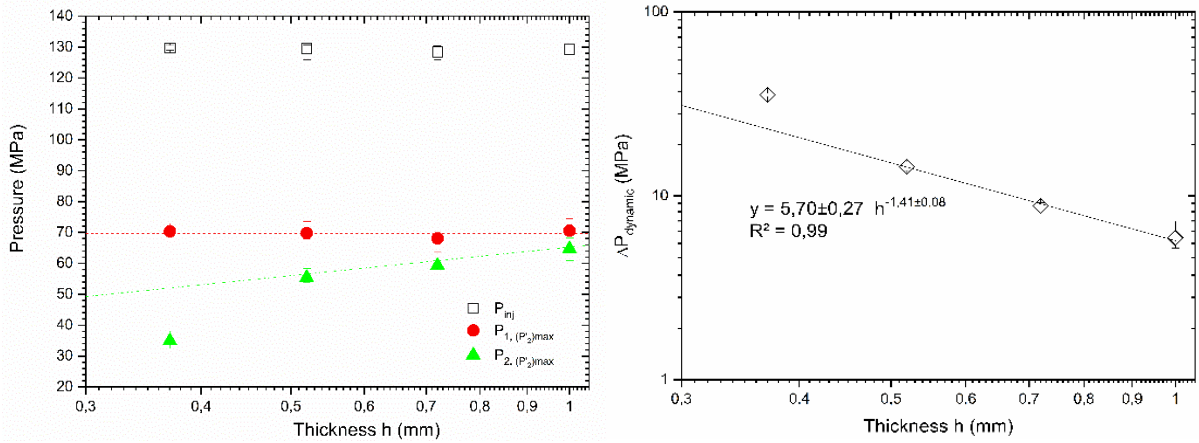

(a) (b)

Figure 4: Evolution of (a) pressure maximum values and b) $\Delta P_{dynamic}$ with cavities thickness for 120°C mold temperature. (Dotted lines = guidelines).

The analysis of the flow rates (Figure 5a) confirms the specific behavior of the 0.37mm cavity. The reduction of the thickness of the cavities leads to the decrease of the flow rates between the two sensors, $Q_{1\text{-}2}$, and between sensor 1 and the end of the cavity, $Q_{dynamic}$, according to power laws. Absolute values of $Q_{1\text{-}2}$ are higher than $Q_{dynamic}$, but the decrease with thickness is of higher intensity. These values are consistent with the flow rate reductions reported by Zhang et al. [15]. In addition, the corresponding average injection speeds $v_{1\text{-}2}$ over 20 mm decrease with the thickness (Figure 5b), whereas $v_{dynamic}$ are constant over the 32.5 mm once h ranges between $1 \geq h \geq 0.52$ mm and shows then an additional decrease for h = 0.37 mm.
Thus, the flow behavior changes with the cavity thickness, probably due to surface effects of higher intensity over the volume effects.

A particular point appears on Figure 5a relative to the intersection of the two trends, corresponding to the fact that $Q_{1\text{-}2}$ is equal to $Q_{dynamic}$ or that $v_{1\text{-}2} = v_{dynamic}$. Knowing that $Q_{dynamic}$ cannot be greater than $Q_{1\text{-}2}$, this assumption allows us to define a critical point, called $h_{critical}$ in the rest of this article, for which surface effects becomes stronger and not anymore neglectable compared to the volume effects. The role of the mold/polymer interface requires thus a special attention to fill thin-wall cavities, by promoting the sliding of macromolecular chains in contact with the mold. Such a phenomenon can be generated by surface coatings on the tools [23] or by the addition of slip agents in the polymer formulation [24]. In the next paragraph, we will then modify the interface conditions by changing the mold temperature and study the flow behavior of the copolymer.

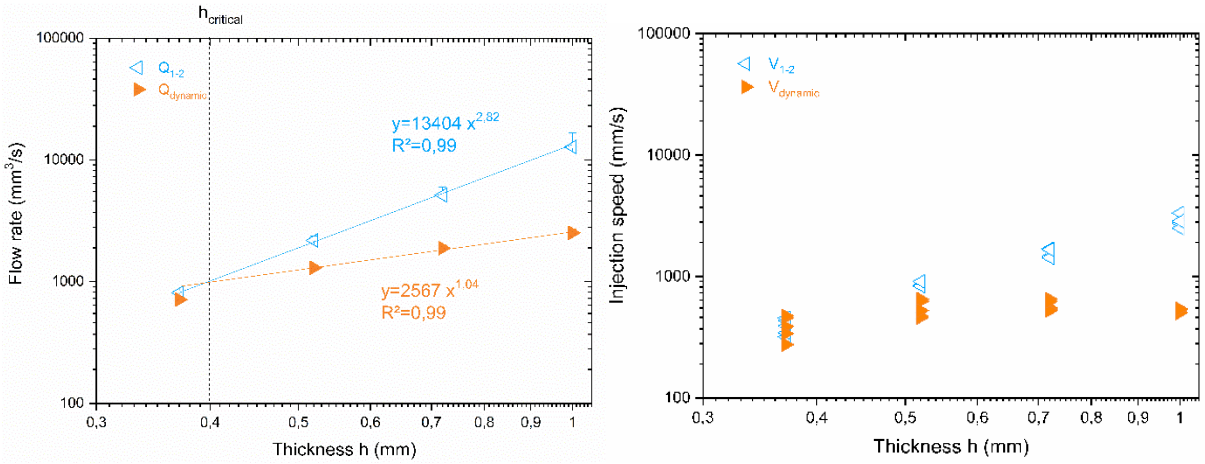

(a) (b)

Figure 5: a) Evolution of the flow rates $Q_{1\text{-}2}$ & $Q_{dynamic}$ with the cavity thickness for T_{mold} = 120°C and b) Evolution of the velocities $V_{1\text{-}2}$ & $V_{dynamic}$ with the cavity thickness for T_{mold} = 120°C.

3.3 Analysis of cavity filling kinetics from time variations of intra-cavity temperature signals

The Figure 6 shows the temporal evolution of the temperature differential $\Delta T_i(t)$, calculated according to equation (10) for the two positions studied (1 and 2) as a function of the thickness of the cavity and for a mold temperature of 120°C:

$$\Delta T_i(t) = T_i(t) - T_{i_{end}} \quad (10)$$

$T_i(t)$ = the temperature signal and $T_{i_{end}}$ the real cavity temperature at the end of the cycle.

It can be observed for sensor T_1 (Figure 6a), a maximum temperature differential $\Delta T_{1_{max}}$ between 16 and 18 °C, a value increasing with the reduction of the cavity thickness. A local phenomenon seems to occur, accentuating the exothermicity or shear-heating effects related to the filling of the cavity.

At the second sensor level, the maximum temperature differential $\Delta T_{2_{max}}$ are close, with a singular behavior of the 0.37mm exotherm, showing a decrease compared to $\Delta T_{1_{max}}$. This result can be related to the singular pressure drop noted at the sensor 2 for this thickness (see Figure 4b) and the additional exothermic effect noted and illustrated in Figure 7, representing the evolution of ΔT_{rel} as a function of the cavity thickness, according to the following expression :

$$\Delta T_{rel} = \Delta T_{1_{max}} - \Delta T_{2_{max}} \quad (11)$$

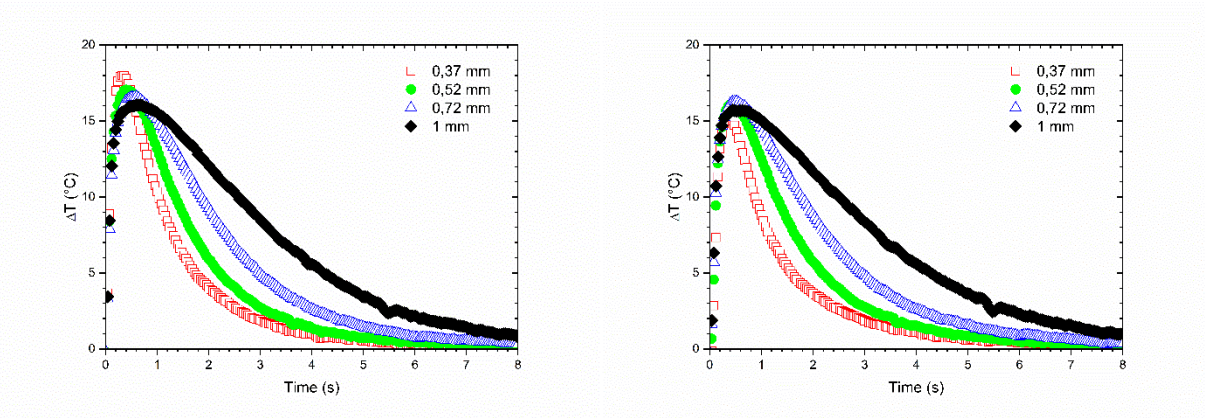

(a) (b)

Figure 6: Temperature variations recorded on the two sensors positions T_1 (a) and T_2 (b), for the different thicknesses with a mold temperature of 120°C.

For cavities thicker than 0.37 mm, the temperature decrease follows a power law with a strong increase of this parameter with the thickness reduction (power = 2.4). Note that the amplitude of this parameter remains contained, less than 1°C. For the 0.37 mm thick cavity, an increase of ΔT_{rel} of more than 3°C is observed, with a point located above the trend plotted. To better understand this phenomenon, a study on the influence of the mold temperature on the rheological behavior of the polymer was carried out and the results developed in the next paragraph.

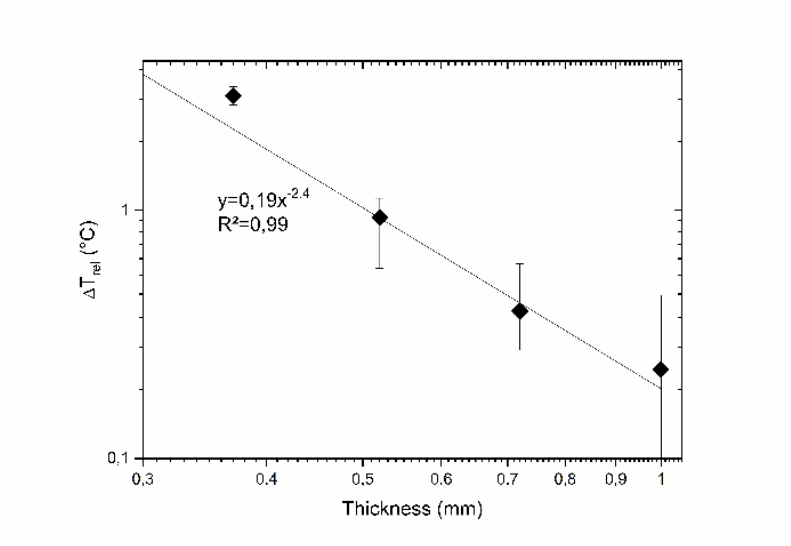

Figure 7: Variations of ΔT_{rel} as function of cavity thickness for T_{mold} = 120°C. The error bars represent the temperature variation over 15 cycles.

3.4 Analysis of the influence of mold temperature on the kinetics of polymer melt filling in cavities of varying sizes

3.4.1 Evolution of $\Delta P_{dynamic}$ and ΔT_{rel} as a function of cavity thickness for different mold temperature

This part is devoted to the study of the influence of the mold temperature on the rheological behavior of polymers in cavities of reduced size. Figure 8 shows the evolution of the calculated pressure drop $\Delta P_{dynamic}$ as a function of the thickness of the cavities for different mold temperatures ranging from 30 to 120°C.

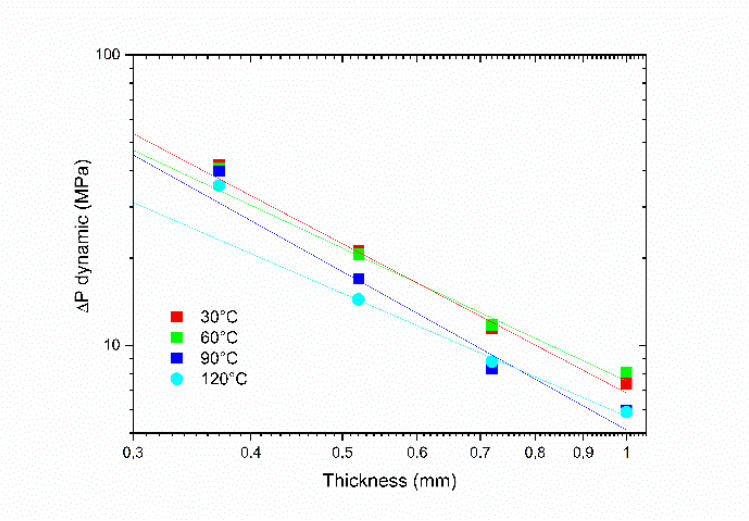

Figure 8: Variations of $\Delta P_{dynamic}$ as function of cavity thickness for different mold temperatures.

We can again observe that this parameter follows a power law, described by equation (9). The values of the parameters a and b and their associated errors (Δa and Δb) have been collected in Table 2, as well as the correlation coefficient R^2 for the different mold temperatures studied.

Table 2 : Values of the parameters a and b and their associated errors (Δa and Δb) from the power law modeling, inspired from equation (9), as a function of the mold temperature. The correlation coefficient R^2 is also given.

Mold temperature (°C)	Parameter a	Standard Error Δa	Parameter b	Standard error Δb	R^2
30	6,9	0,6	-1,7	0,2	0,99
60	7,6	0,7	-1,5	0,2	0,98
90	5,1	1,0	-1,8	0,2	0,95
120	5,7	0,3	-1,4	0,1	0,99

Examination of Figure 8 and the a and b parameter values (Table 2) confirm the power law between the dynamic pressure drop with the increase of cavity thickness, except for the 0.37 mm cavity.

To complete this analysis, we have plotted the evolution of the flow rates $Q_{dynamic}$ and $Q_{1\text{-}2}$ as a function of cavity thicknesses for all mold temperatures studied (Figure 9). We can observe that the mold temperature does not affect the values of Q_{dyn} or $Q_{1\text{-}2}$. The previous power laws highlighted in Figure 5 remain valid, with a power equal to 2.8 for $Q_{1\text{-}2}$ and about 1.0 for $Q_{dynamic}$.

The mold temperature would thus have a negligible effect on the dynamic filling of the cavity in the case of this copolymer; this result is remarkable because it was not predictable.

As observed previously, we can again note the singular behavior of the 0.37 mm thick cavity, with flow values below the prediction given by the fits, highlighting an additional phenomenon occurring in the case of the thinner cavity. The intersection between the two trends allows one more time to define the critical thickness $h_{critical}$ where the surface and interface phenomena exceed the volume phenomena. More generally, we can conclude that this arises once flow length is higher than 77 times the thickness. This value is confirmed for the different mold temperatures and can be related to the change of flow type in micro-cavities, giving an average value of $L/h_{critical} \approx 77 \pm 7$, from the results reported in Table 3.

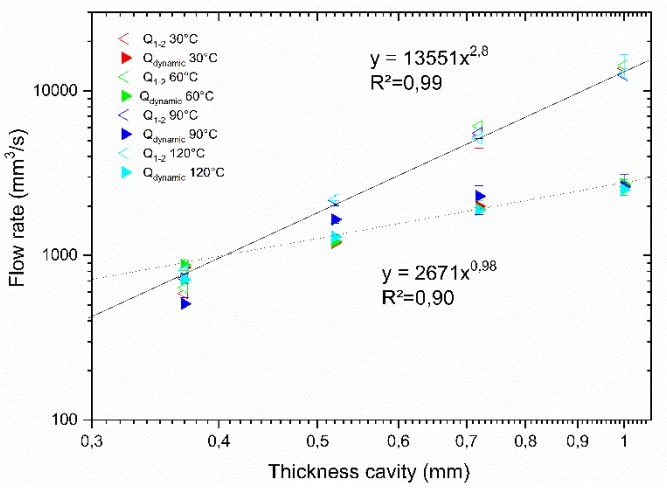

Figure 9: Evolution of the flow rates $Q_{1\text{-}2}$ & $Q_{dynamic}$ as a function of cavity thickness h for different mold temperatures (colors for 30, 60, 90 and 120°C).

Table 3 : Values of critical thicknesses $h_{critical}$ and critical aspect ratio, $L/h_{critical}$ as a function of mold temperatures.

T(°C)	$h_{critical}$	$L/h_{critical}$
30	0,42	77
60	0,40	81
90	0,48	68
120	0,40	81
Average	0.425	77

The last part of this study will consist in verifying the influence of the mold temperature on the intracavity thermal behavior, measured with the temperature probes T_1 and T_2. Figure 10 presents the evolution of ΔT_{rel} as a function of the mold temperature for the different thicknesses studied.

Regarding the evolution of the local temperature with the mold temperature (Figure 10) the temperature variations between the two sensors are almost identical and not much that 1°C, considering that error bars. This means that the thermal conditions within the polymer flow is equilibrated and that the mold surface temperature has a negligible impact on the overall temperature conditions within the flow. This is clearly not the case for the 0.37 mm cavity thickness, where the temperature variation in the cavity decreases linearly with the increase of mold temperature, confirming additional heat loss. For that specific thickness, the mold temperature affects the temperature within the polymer volume, and lead to an additional energy loss.

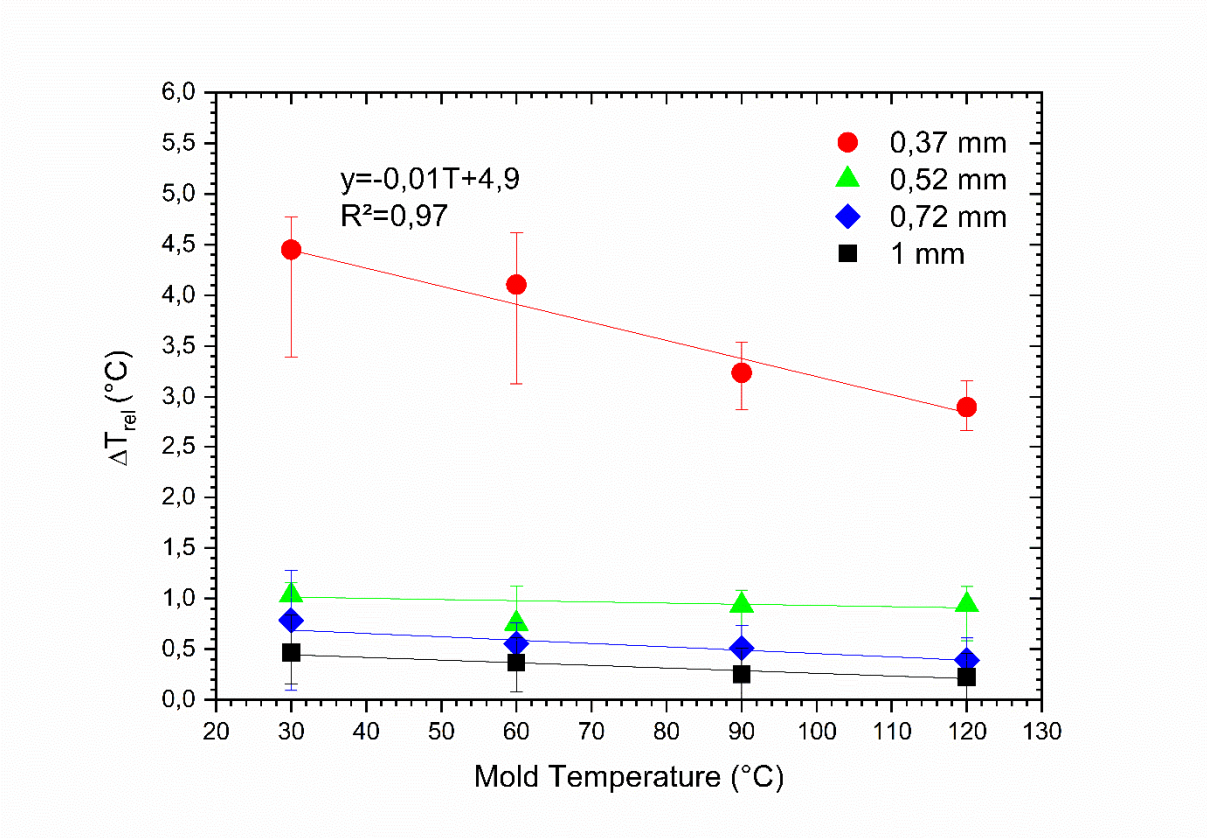

Figure 10: Variation of ΔT_{rel} with mold temperatures for different cavities thickness.

To go further in the understanding of this dissipative phenomena, we compared the evolution of the pressures $P_{1,(P'2)max}$ and $P_{2,(P'2)max}$ for the cavities of 1 and 0.37 mm as a function of the inverse of the mold temperature T_{mold} (Figure 11).

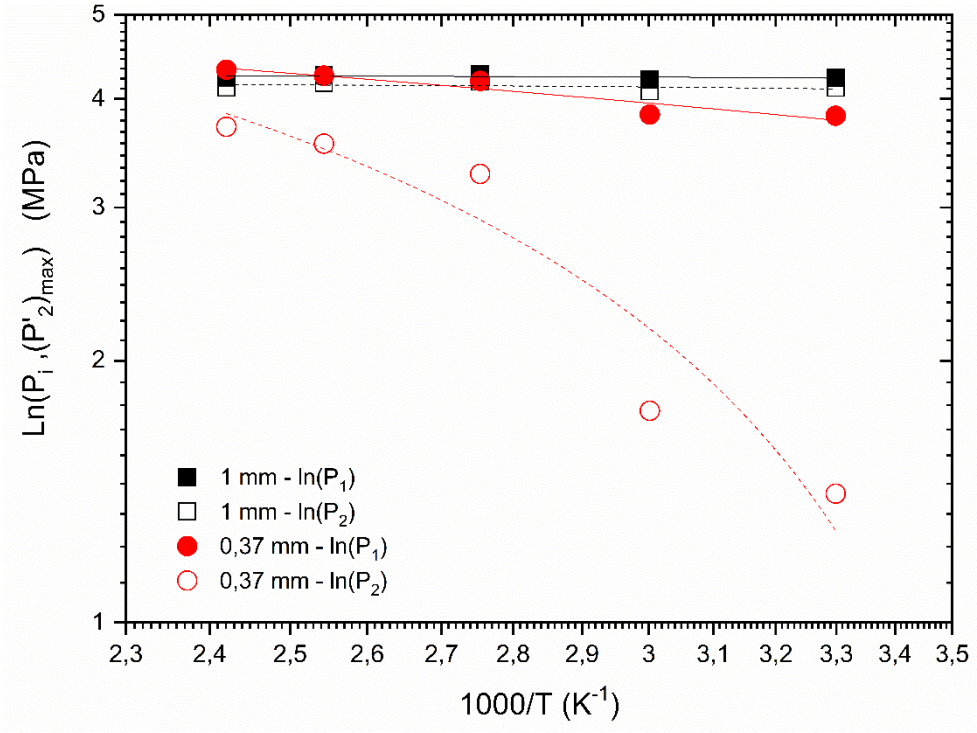

Figure 11: Evolution of the logarithm of maximum pressures $\mathbf{P_{1_{max}}}$ and $\mathbf{P_{2_{max}}}$ for the cavities of 1 and 0.37mm as a function of $1000/T_{mold}$.

For the 1 mm thick cavity, no dependence between pressure and temperature is found, in agreement with the previous results. On the contrary, for the 0.37mm thick cavity, a behavior following an Arrhenius law is observed at the sensor 1 with an activation energy close to 5 ± 1 kJ/mol. A higher activation energy of 20 ± 3kJ/mol is measured from the sensor 2, confirming the additional dissipative phenomenon occurring at the mold/polymer interface and leading to the stronger pressure drops observed for this cavity. The volume effects leading the rheological behavior within the copolymer flow in the cavity is then countered by the surface effects taking the ascendancy over the first ones. The *in-situ* measurements of pressure and temperature in the cavities during the injection of polymers are excellent markers of the rheological phenomena occurring during the dynamic phase.

4 Conclusions

The rheological behavior of an Ethylen-Norbornen copolymer injected in cavities of thickness ranging from 1 to 0.37mm has been studied, thanks to the use of "la Rotonde", a tool integrating pressure and temperature sensors. It has focused on a time scale characteristic of the dynamic filling phase of injection. Based on the data acquisition, a specific methodology has been proposed, based on the time derivative of the pressure signals, measured at two positions along the flow.

The in-situ measurements show that pressure drops increase with decreasing thickness according to a power law, which goes along with a decrease of the flow rates. A specific behavior was observed for the smallest cavity (0.37mm), explaining the impossibility to fill completely cavities of lower thickness (including 0.27mm), whatever the injection conditions used. A critical thickness has been identified around $h_{critical} = 0.42 \pm 0{,}04$ mm and being independent of the mold temperature. This is characteristic of additional dissipation phenomena occurring below this value and appearing once

L/h is higher than the critical ratio $L/h_{critical} = 77 \pm 7$ for any temperature. Therefore, the dissipative and thermally activated phenomena are observed for this critical thickness with an increasing activation energy along the flow path.

Such results are certainly essential data to optimize the dimensions and shapes of the objects to be molded and to avoid local phenomena leading to defects on the injected objects or process-induced modifications of the polymers properties. Therefore, in the aim of shifting this critical value to lower ones and thus allow the molding of parts of smaller dimensions or better controlled quality, different strategies could be followed. One of them could rely on the synthesis of sliding agents blended with polymers or else by using surface coatings on tools promoting the sliding of macromolecular chains at its interface, subjects under study.

Acknowledgements

The authors greatly acknowledge Philippe Vuillermoz and Sylvain Clerc for the design and development of the experimental apparatus “La Rotonde”, as well as David Baud from CT IPC for the set-up of the injection molding experiments. The authors thank Nicolas Charvin from LEPMI for its valuable help for setting up the data acquisition system.

Bibliography

[1] Plastic Market Size, Share & Trends Analysis Report By Product (PE, PP, PU, PVC, PET, Polystyrene, ABS, PBT, PPO, Epoxy Polymers, LCP, PC, Polyamide), By Application, By End-use, By Region, And Segment Forecasts, 2021 – 2028, Grand View Research Inc., 230 pages, 2021 [Accessed 20 July 2021].
[2] Griffiths CA, Rees A, Kerton RM, Fonseca OV. Temperature effects on DLC coated micro moulds. Surf Coat Technol 2016; 307: 28-37. https://doi.org/10.1016/j.surfcoat.2016.08.034
[3] Giboz J, Copponnex T, Mélé P. Microinjection molding of thermoplastic polymers: A review. J Micromech Microeng 2007; 17: R96–R109. https://doi.org/10.1088/0960-1317/17/6/R02.
[4] Masato D, Sorgato M, Lucchetta G. Analysis of the influence of part thickness on the replication of micro-structured surfaces by injection molding. Mater Des 2016; 95: 219-24. https://doi.org/10.1016/j.matdes.2016.01.115.
[5] Gamonal-Repiso P, Sánchez-Soto M, Santos-Pinto S, Maspoch ML. Improvement of the replication quality of randomly micro-textured injection-moulding components using a multi-scale surface analysis. J Manuf Process 2019; 42: 67-81. https://doi.org/10.1016/j.jmapro.2019.04.010.
[6] Giboz J, Spoelstra AB, Portale G, Copponnex T, Meijer HEH., Peters GWM, Mélé P. On the origin of the ''core-free'' morphology in microinjection-molded HDPE. J Pol Sci Part B: Polym Phys 2011; 49: 1470-78. https://doi.org/10.1002/polb.22332.
[7] Giboz J, Vite M, Bec S, Loubet JL, Copponnex T, Mélé P. Observation of specific polymer morphologies in a microinjection moulded part. 4M2010: Proceedings of the 7th International conference on Multi-Material Micro Manufacture 2010; 103-106.
[8] Yao D, Kim B. Scaling Issues in Miniaturization of Injection Molded Parts. J Manuf Sci Eng 2004; 126: 733-739. https://doi.org/10.1115/1.1813479.
[9] Mélé P, Giboz J, Micro-injection molding of thermoplastic polymers: proposal of a new constitutive law as function of the aspect ratios. J Appl Polym Sci 2017; 134: 45719. https://doi.org/10.1002/app.45719.
[10] Vasco JC, Maia JM, Pouzada AS. Thermo-rheological behaviour of polymer melts in microinjection moulding. J Micromech Microeng 2009; 19: 105012. https://doi.org/10.1088/0960-1317/19/10/105012.

[11] Deng P, Zhang J, Liu F, Liu K, Liu H, Zhang L. Shear-Induced Flow Behavior of Three Polymers in Different Size Dies. J Macromol Sci Part B 2013; 52: 651-661. https://doi.org/10.1080/00222348.2012.720171.
[12] Sorgato M, Masato D, Lucchetta G, Orazi L. Effect of different laser-induced periodic surface structures on polymer slip in PET injection moulding. CIRP Ann - Manufacturing Technology 2018; 67: 575–578. https://doi.org/10.1016/j.cirp.2018.04.102.
[13] Trotta G, Stampone B, Fassi I, Tricarico L. Study of rheological behaviour of polymer melt in micro injection moulding with a miniaturized parallel plate rheometer, Polym Testing 2021; 96: 107068. https://doi.org/10.1016/j.polymertesting.2021.107068.
[14] Vera J, Contraires E, Brulez AC, Larochette M, Valette S, Benayoun S. Wetting of polymer melts on coated and uncoated steel surfaces. Appl Surf Sci 2017; 410: 87 – 98. https://doi.org/10.1016/j.apsusc.2017.02.067.
[15] Zhang N, Gilchrist MD. Characterization of thermo-rheological behavior of polymer melts during the micro injection moulding process, Polym Test 2012; 31: 748–758. https://doi.org/10.1016/j.polymertesting.2012.04.012.
[16] Masato D, Sorgato M, Babenko M, Whiteside B, Lucchetta G. Thin-wall injection molding of polystyrene parts with coated and uncoated cavities. Mater Des 2018; 141: 286-295. https://doi.org/10.1016/j.matdes.2017.12.048
[17] Surace R, Sorgato M, Bellantone V, Modica F, Lucchetta G, Fassi I. Effect of cavity surface roughness and wettability on the filling flow in micro injection molding. J Manuf Processes 2019, 43: 105-111. https://doi.org/10.1016/j.jmapro.2019.04.032.
[18] Baruffi F, Gülçür M, Calaon M, Romano JM, Penchev P, Dimov S et al. Correlating nano-scale surface replication accuracy and cavity temperature in micro-injection moulding using in-line process control and high-speed thermal imaging. J Manuf Processes 2019; 47: 367–381. https://doi.org/10.1016/j.jmapro.2019.08.017.
[19] Masato D, Sorgato M, Batal A, Dimov S, Lucchetta G. Thin-Wall Injection molding of polypropylene using molds with different Laser-Induced Periodic Surface Structures. Polymer engineering and science 2019; 59: 1889-1896. https://doi.org/10.1002/pen.25189.
[20] Gülçür M, Brown E, Gough T, Romano JM, Penchev P, Dimov S et al. Ultrasonic micromoulding: Process characterisation using extensive in-line monitoring for micro-scaled products. J Manuf Processes 2020; 58: 289-301. https://doi.org/10.1016/j.jmapro.2020.08.033.
[21] Guerrier P, Tosello G, Hattel JH. Flow visualization and simulation of the filling process during injection molding. CIRP J Manuf Sci Technol 2017; 16: 12-20. https://doi.org/10.1016/j.cirpj.2016.08.002.
[22] Nunes PS, Ohlsson P, Ordeig O , Kutter J. Cyclic olefin polymers: emerging materials for lab-on-a-chip applications. Microfluid Nanofluid 2010; 9: 145-161. https://doi.org/10.1007/s10404-010-0605-4.
[23] Mélé P, Giboz J, Fugier P, Baud D, Vuillermoz P. Empreinte pour outillage de plasturgie et procédé de plasturgie. Patent FR3042146 & CH711636. Priority date 2015-10-13.
[24] Nourdine A, Giboz J, Le Brouster R, Dubelley F, Carrier S, Tenchine L, Mele P, Tailored fluorinated oligo-polystyrene as efficient additive for the hydrophobicity/oleophobicity improvement of styrenic polymers. Polym J 2021, 159 : 110712. https://doi.org/10.1016/j.eurpolymj.2021.110712.